Activation and In Situ Ethylene Polymerization on Silica-Supported Ziegler-Natta Catalysts

Activation And In Situ Ethylene Polymerization On Silica-Supported Ziegler-Natta Catalysts

Elena Groppo[1,*], Kalaivani Seenivasan[1], Erik Gallo[1,2], Anna Sommazzi[3], Carlo Lamberti[4,5], Silvia Bordiga[1]

[1]Department of Chemistry, INSTM and NIS Centre, University of Torino, Via Quarello 15, 10135 Torino, Italy.

[2]European Synchrotron Radiation Facility, 6 Rue Jules Horowitz, 38043 Grenoble, France.

[3]Versalis – Novara Research Center, Istituto Eni Donegani, Via Fauser, 4 - 28100 Novara, Italy.

[4]Department of Chemistry, INSTM and CrisDi Centre, University of Torino, Via Giuria 7, 10125 Torino, Italy

[5]Southern Federal University, Zorge Street 5, 344090 Rostov-on-Don, Russia.

ABSTRACT: The structural, vibrational and electronic properties of silica-supported Ziegler-Natta catalysts industrially relevant for polyethylene production were investigated in details by means of a multi-technical approach, at each step of catalyst preparation - including pre-catalyst activation. In the pre-catalyst, the $TiCl_x$ phase is mainly grafted to the silica surface, and almost independent of the supported $MgCl_x$ phase. However, the subsequent activation by means of an aluminum-alkyl compound causes important changes to both, the supported $MgCl_x$ phase and the $TiCl_x$ phase. The resulting catalyst is entirely reconstructed, so that most of the titanium sites are detached from the silica surface and in interaction with a highly dispersed $MgCl_2$ phase, thus mimicking the most famous and highly investigated Ziegler-Natta catalysts (not silica-supported). For the first time, the catalyst performances were monitored by means of in situ FT-IR spectroscopy in transmission mode, simulating industrially significant polymerization conditions (i.e. ethylene is fed onto the catalyst in the presence of the activator and of the solvent). These results demonstrate that it is now possible to achieve a complete description at a molecular level of all the constituents of Ziegler-Natta catalysts, at each step of the catalyst preparation.

KEYWORDS: Ziegler-Natta catalysts; polyethylene; polymerization; in situ spectroscopic techniques; silica.

1. INTRODUCTION

Heterogeneous Ziegler-Natta catalysts for polyolefins production are among the most employed and versatile catalysts in the chemical industry, and probably those having the largest impact not only in science, but in everyday life. The extraordinarily large number of polymer architectures today available and the remarkable rapid progress in polyolefin technology, are closely associated with the catalyst's development and innovation in process technology. Since their discovery in 1960s, heterogeneous Ziegler-Natta catalysts have progressed enormously, making it possible to produce advanced polyolefin materials having tailored properties. Today, Ziegler-Natta catalysis allows a precision synthesis of polyolefins, based on the exact assembly of the olefin monomers at the nano-scale through the intervention of the active catalytic sites.[1-3]

Most of the breakthrough in this field was the result of a trial-and-error approach, commonly adopted not only in the chemical industries involved in polyolefin production, but also in the academic laboratories. The opposite method to improve the catalyst's performances, that is a full elucidation of the catalyst's structure by means of combined spectroscopic and structural experimental methods, is much less widespread.[4] In situ investigation of heterogeneous Ziegler-Natta catalysts is hampered by two main problems: i) the active species are only a few of a number (whereas the majority are spectators), which altogether determine the behavior of the catalytic system; ii) the ease of contamination, which implies that comparing or combining data obtained in different laboratories is risky.[5] For these reasons, so far most of the experimental investigations on heterogeneous Ziegler-Natta systems were focused on the pre-catalyst only, i.e. the system before interaction with the activator, usually an aluminum-alkyl compound. Pre-catalysts are simpler in chemical composition and much less sensitive to contamination. Although the properties of the pre-catalyst might have an influence on those of the catalyst, it was demonstrated that the activator causes a substantial transformation in the pre-catalyst, involving all the components and not only the active phase.[5-8] Therefore, elucidation of the catalyst structure requires the ability to investigate the system in the presence of the activator, if not in the presence of both the activator and the olefin monomer, i.e. in reaction conditions.

In situ and operando studies are nowadays common in catalysis and have provided substantial progresses in the understanding of the catalyst's performances in many important catalytic processes.[9-19] The experimental tools have progressed enormously in the last years, allowing to investigate catalysts in action, even in extreme conditions (high temperature, high pressure, etc.) and with increasing time- and space-resolution. Unfortunately, application of these methods to Ziegler-Natta catalysts is still at the beginning.[5] Among the few studies on Ziegler-Natta catalysts in action, we mention the in situ optical observation of growing polypropylene particles on heterogeneous Ziegler-Natta catalysts.[20,21] Although fascinating, these results give information on the kinetics of the polymerization only, but they are not informative about the structure of the active sites on a molecular scale. A few efforts in this direction were attempted by means of surface science methods applied to planar models of Ziegler-Natta catalysts. Thune and his group

developed a smart experimental set-up which allows to monitor each step of catalyst preparation (including pre-catalyst activation) and olefin polymerization, by means of in situ ATR-IR spectroscopy.[22-25] Very recently, a detailed characterization of potential catalytically active sites in an activated $MgCl_2$-supported industrial Ziegler–Natta catalyst was achieved also by means of advanced EPR techniques[26] that, however, are completely silent towards all other catalyst's constituents. Hence, we could safely say that, despite these little efforts, the structural and electronic properties of the titanium active sites and their relation with all the catalytic body in heterogeneous Ziegler-Natta catalysts remain substantially a black-box.

Recently, we have been involved in a systematic investigation of heterogeneous Ziegler-Natta catalysts based on titanium and magnesium chloride tetrahydrofuranates, which have been patented in the early 1970s,[27,28] and are facing a new youth in the very last years because of the increasing attention of academic laboratories.[5,7,8,29-31] In our previous works we have demonstrated the potential of a multi-technique approach in unraveling the nature of the active $TiCl_x$ phase in catalysts obtained by reacting together titanium and magnesium chloride tetrahydrofuranate precursors and the aluminum-alkyl activator.[7,8] The investigation is more complex when the $TiCl_x$ and $MgCl_x$ phases are simultaneously supported on dehydroxylated silica in presence of tetrahydrofuran. This catalyst was developed in the 1980s by a group of scientists from Union Carbide Corporation in order to be used in the UNIPOL process to produce high density polyethylene.[32-38] The use of polymer-grade dehydroxylated silica as a support in polymerization catalysts is nowadays quite common, since it provides a larger surface area along with a good control of the polymer morphology.[38-42] Although silica is often described just as a template to produce polyethylene particles having the right particle size and particle size distribution suitable for gas-phase processes, it is now well documented that it plays also an active role in defining the properties of the catalyst as a whole.[5,43-46] The simpler SiO_2/Ti system (where Ti stands for $TiCl_4(thf)_2$ precursor, thf = tetrahydrofuran) has been the subject of a previous investigation by means of X-ray Powder Diffraction (XRPD), FT-IR, UV-Vis, X-ray Absorption Spectroscopy (XAS) and valence-to-core X-ray Emission Spectroscopy (vtc-XES) techniques.[47] We have demonstrated that the synergic combination of these techniques allows to reach a complete scenario on the properties of the supported titanium phase. Herein we proceeded the investigation by looking at the SiO_2/TiMg pre-catalyst (where Ti stands for $TiCl_4(thf)_2$ precursor, and Mg for the $MgCl_2(thf)_{1.5}$, precursor, thf = tetrahydrofuran), and at the catalyst originated after interaction with the aluminum-alkyl activator (TOAl = trioctyl-aluminum). The whole arsenal of characterization techniques cited above allowed us to obtain information on the role of the activator in constructing the catalytically active phase, not only in terms of titanium sites, but also considering the $MgCl_x$ phase as well as the thf donor and the silica support. Ultimately, we looked at the catalyst in action by means of in situ FT-IR spectroscopy, mimicking industrially significant ethylene polymerization conditions.

2. EXPERIMENTAL

2.1 Materials. Davison sylopol silica 955 grade (surface area = 276 m^2/g, pore volume = 1.76 ml/g, average pore diameter = 266 Å, average particle size = 31 μm) was used as support, after a pre-treatment in air at 550°C for 8 hours, followed by a cooling step carried out in nitrogen atmosphere. $TiCl_4(thf)_2$ and $MgCl_2(thf)_{1.5}$ precursors were synthesized following the recipe reported elsewhere.[48] The silica-supported samples were prepared following a procedure similar to that adopted in our previous work,[47] and in agreement with that reported in the original patents.[32,33] Briefly, the two precursors were dissolved in dry tetrahydrofuran (thf) and impregnated on dehydroxylated SiO_2 in controlled atmosphere, using Schlenk technique, resulting in titanium loading of 4 wt% and magnesium loading of 1.6 wt%. The excess of the solvent was further removed by gently heating the sample up to ca. 60 °C. The resulting pre-catalyst will be called hereafter SiO_2/TiMg. Single-phase silica-supported samples having the same amount of titanium (or magnesium) were prepared following the same method; these samples will be referred in the following as SiO_2/Ti and SiO_2/Mg.

The catalyst was prepared from pre-catalyst (in the form of powder or pellet, depending on the measurement) upon impregnation with trioctylaluminum (TOAl, Aldrich, 25% diluted in heptane, approximate Al/Ti ratio of 10:1), inside a N_2-filled glove-box. This preparation step was always accomplished immediately before the measurement in order to prevent catalyst deactivation. The so prepared catalyst (hereafter, SiO_2/TiMg/TOAl) was then transferred into the measurement cell. For in situ FT-IR measurements during polymerization, deuterated ethylene (equilibrium pressure P_{C2D4} = 100 mbar) was directly dosed into the reaction cell, after the evacuation of N_2. This procedure was found to be critical, because removal of N_2 may cause also a partial removal of the heptane solvent followed by a fast deactivation of the catalyst. For this reason, evacuation of N_2 was performed by keeping the catalyst cold by means of a liquid nitrogen cold point. Then the catalyst was allowed to warm up to room temperature, followed by dosage of d-ethylene into the measurement cell.

Table 1 contains a summary of all the samples investigated in this work, of the short labels, and of the corresponding entries as adopted in the Figures.

Table 1. Summary of all the samples investigated in this work.

Entry	Short label	Full name
0	Mg	$MgCl_2(thf)_{1.5}$
1	SiO_2/Mg	$SiO_2/MgCl_2(thf)_{1.5}$
1'	SiO_2/Ti	$SiO_2/TiCl_4(thf)_2$
2	SiO_2/TiMg	$SiO_2/TiCl_4(thf)_2/MgCl_2(thf)_{1.5}$
3	SiO_2/TiMg/TOAl	$SiO_2/TiCl_4(thf)_2/MgCl_2(thf)_{1.5}$ + TOAl
4	SiO_2/TiMg/TOAl + C_2D_4	$SiO_2/TiCl_4(thf)_2/MgCl_2(thf)_{1.5}$ + TOAl + C_2D_4

2.2 Techniques. *X-ray Powder Diffraction (XRPD).* X-ray Powder Diffraction patterns were collected with a PW3050/60 X'Pert PRO MPD diffractometer from PANalytical working in Debye-Scherrer geometry, using as source a Cu anode filtered by a Ni foil to attenuate the Kβ line and focused by a PW3152/63 X-ray mirror (λ = 1.5409 Å). The samples were measured as powders inside a 0.8 mm boron-silicate capillary sealed in inert atmosphere.

X-ray Absorption Spectroscopy (EXAFS and XANES). Ti K-edge EXAFS spectra were collected at the BM26A beamline

(DUBBLE) at the European Synchrotron Radiation Facility (ESRF, Grenoble, F).[49] The white beam was monochromatized using a Si(111) double crystal; harmonic rejection was performed by using silicon mirrors. Due to the fact that Ti K-edge was the lowest energy feasible at DUBBLE and that the samples investigated were quite inhomogeneous, it was mandatory to develop a full feedback strategy for keeping full beamline flux whilst keeping beam delivery at a fixed exit point. EXAFS scans at low energies bring out the worst of the monochromators alignment issues and exit beam swing. To this purpose, two feedback systems were implemented:[50] i) a position feedback, to keep beam delivered at a single vertical position within a 2 micrometer window (it acts on the mirrors) within the whole EXAFS scan; and ii) a I_0 feedback, to keep I_0 optimal throughout the EXAFS scan (it acts on the second crystal of the monochromator).

Due to titanium dilution and to the absorbing nature of the support, EXAFS spectra were collected in fluorescence mode, by means of a 9 elements germanium monolithic detector. The intensity of the incident beam was monitored by an ionization chamber filled with 1.2 bar of 5% N_2 – 95% He mixture, resulting in a 10% efficiency in the middle of the EXAFS scan). All the samples were manipulated in controlled atmosphere, inside an argon-filled glove-box. The samples were measured in the form of self-standing pellets, inside a home-made quartz cell equipped with two kapton windows. Argon was removed from the cell before the measurement, because it absorbs a high fraction of the incoming beam at the low energy of Ti K-edge. For the catalyst in presence of TOAl, care was taken to remove argon by keeping cold the sample, to avoid removal of TOAl and/or heptane, and consequent deactivation of the catalyst.

The XANES part of the spectra was acquired with an energy step of 0.4 eV and an integration time of 2s/point. The EXAFS part of the spectra was collected up to 12 $Å^{-1}$ with a variable sampling step in energy, resulting in a constant sampling step in k-space of $\Delta k = 0.05$ $Å^{-1}$, and an integration time that linearly increases as a function of k from 5 to 20 s/point to account for the low signal-to-noise ratio at high k values. For each sample, at least four equivalent EXAFS spectra were acquired and averaged before the data analysis. The extraction of the $\chi(k)$ functions was performed using Athena program.[51] Once extracted, the k^3-weighted $\chi(k)$ functions were Fourier transformed in the $\Delta k = 2.0 – 10.0$ $Å^{-1}$ range. This Δk interval has been selected in a conservative way, i.e. in order to avoid the introduction of false signals in the FT. The fits were performed in R-space (in the $\Delta R = 1.0 – 3.0$ Å range, resulting in a maximum number of independent parameters $2\Delta k\ \Delta R/\pi$ larger than 10), using the Arthemis program.[51] Phase and amplitudes were calculated by FEFF6.0 code.[52]

X-ray Emission Spectroscopy (XES). XES experiments were performed at beamline ID26 of the European Synchrotron Radiation Facility (ESRF, France). The incident energy ($\hbar\Omega$) was selected by means of a pair of cryogenically cooled Si(311) single crystals (higher harmonics were suppressed by three Si mirrors operating in total reflection). The fluorescence photon energy ($\hbar\omega$) was selected using an emission spectrometer working in vertical Rowland Geometry employing five Ge(331) spherically bent analyzer crystals of radius 1000 mm covering 70-110 degrees in the horizontal scattering plane. The emitted photons were detected using an avalanche photo-diode. The total energy bandwidth was 0.9 eV (as determined from the full width at half maximum of the elastically scattered peak). The sample to crystal analyzer to photodiode path undergone by the Ti fluorescence photons occurs inside a slightly over-pressured He bag limiting the X-ray absorption. The samples were found to suffer from radiation damage on a fast timescale (about 10 s), due to the high photon flux adopted during vtc-XES measurements (more than 10^{12} photons per second). To circumvent this problem, each point of the vtc-XES spectrum was collected on a different sample spot irradiated for 2 seconds, and the intensity was normalized to the total fluorescence-yields signal, integrated over the Ti K_α and K_β lines, recorded with a solid-state detector. The micrometric size of the beam and the large size of the sample (4 cm^2) allowed us to have sufficient fresh points on the sample to collect a full vtc-XES spectrum. As for XAS, the samples were measured in the form of self-supporting pellets prepared inside a glove-box and placed inside a cell with kapton windows. Also in this case, the cell was outgassed before measurements in order to remove argon, which absorbs most of the beam at this low energy. The background of the vtc-XES spectra, due to the $K\beta_{1,3}$ peak tail, was subtracted according to the procedure discussed in Ref. [53,54]. Preliminary DFT calculations were performed within the one electron approximation using the ORCA 2008 code.[55]

Diffuse Reflectance UV-Vis Spectroscopy (DR UV-Vis). UV-Vis-NIR spectra were collected in Diffuse Reflectance mode on a Cary5000 Varian spectrophotometer. All the samples were measured in the powdered form inside a cell having an optical window (suprasil quartz) and allowing to perform measurements in controlled atmosphere.

IR spectroscopy (Mid-IR and Far-IR). FT-IR spectra in the Mid-IR region were acquired in transmission mode on a Bruker Vertex70 spectrophotometer equipped with a MCT detector, at a resolution of 2 cm^{-1}. The samples were measured in the form of self-supporting pellets inside a quartz cell equipped with KBr windows in controlled atmosphere. Far-IR spectra were collected at a resolution of 4 cm^{-1} with the same instrument, after changing the optics (Si beam splitter) and the detector (Far-IR DTGS). The samples were mixed with paraffin (which is perfectly transparent in the Far-IR region) inside the glove-box and measured in form of pellets. Paraffin protects the samples from air contamination at least for the time necessary to perform the measurement (a few minutes).

3. RESULTS AND DISCUSSION

3.1 From the pre-catalyst to the catalyst. *Identification of the crystalline phases.* The XRPD patterns of the SiO_2/TiMg pre-catalyst and of the catalyst are show in Figure 1, together with those of the magnesium chloride tetrahydrofuranate precursor and of SiO_2/Mg. When the titanium and magnesium chloride tetrahydrofuranate precursors are simultaneously present on silica (curve 2), well defined diffraction peaks are observed in the XRPD pattern, overlapped to the broad peak due to amorphous silica ($2\theta = 22°$). The sharp peaks are characteristic of the crystalline magnesium precursor (curve 0).[7] It is important to notice that when the two titanium and magnesium chloride tetrahydrofuranate precursors are reacted together in thf solution in absence of silica, a micro-crystalline Ti-Mg

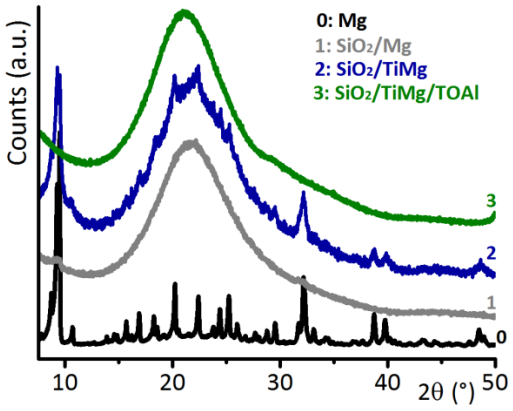

Figure 1. XRPD patterns (λ = 1.5409 Å) of magnesium chloride tetrahydrofuranates precursor (curve 0), SiO_2/Mg single-phase sample (curve 1), SiO_2/TiMg pre-catalyst (curve 2), and SiO_2/TiMg/TOAl catalyst (curve 3). The patterns have been vertically translated for clarity.

ionic complex is formed, which is characterized by a peculiar XRPD pattern.[7,28,34,35,56,57] Such a complex is not observed in the present case. This observation clearly shows that silica does not simply act as a template to host the same catalytic phase that would be formed in its absence, but plays an active role in the construction of the catalyst.

Interestingly, in the presence of the magnesium precursor only (in the same amount) no diffraction peaks are observed in the XRPD pattern (Figure 1, curve 1). This suggests that in the presence of the titanium phase the dispersion of the Mg phase on silica decreases. In order to further clarify this phenomenon, a different bi-metallic pre-catalyst was prepared by following a double impregnation method: the magnesium chloride tetrahydrofuranate precursor was added at first, followed by impregnation of the titanium precursor. The resulting XRPD pattern (not reported) was the same as for the SiO_2/TiMg sample prepared via a single impregnation procedure. Thus, we conclude that the titanium chloride tetrahydrofuran precursor has a better affinity towards the silica than the magnesium precursor. However, the XRPD data do not give any information about the localization of the $TiCl_x$ phase on the silica surface and its eventual interaction with the $MgCl_x$ phase in the SiO_2/TiMg pre-catalyst.

Addition of TOAl to the pre-catalyst causes a remarkable change in the diffraction pattern (Figure 1, curve 3): the peaks identifying the crystalline magnesium-containing phase are no more observed, and only the broad halo due to amorphous silica remains. Hence, we conclude that the co-catalyst interacts strongly with the silica-supported $MgCl_x$ phase. Again, no information can be obtained on the structure of the active $TiCl_x$ phase.

Vibrational properties. Successively, FT-IR spectroscopy was employed to investigate the vibrational properties of both the pre-catalyst and the catalyst. Indeed, FT-IR spectroscopy is a precious technique to evaluate the occurrence of Ti grafting through surface ≡SiOH groups, as previously demonstrated by some of us for the single phase SiO_2/Ti sample,[47] and as reported in literature for the similar $SiO_2/TiCl_4$ system,[58-63] and for several organometallic complexes of general formula X_xML_n (where M = transition metal, X = halogen, and L = ligand).[64-71]

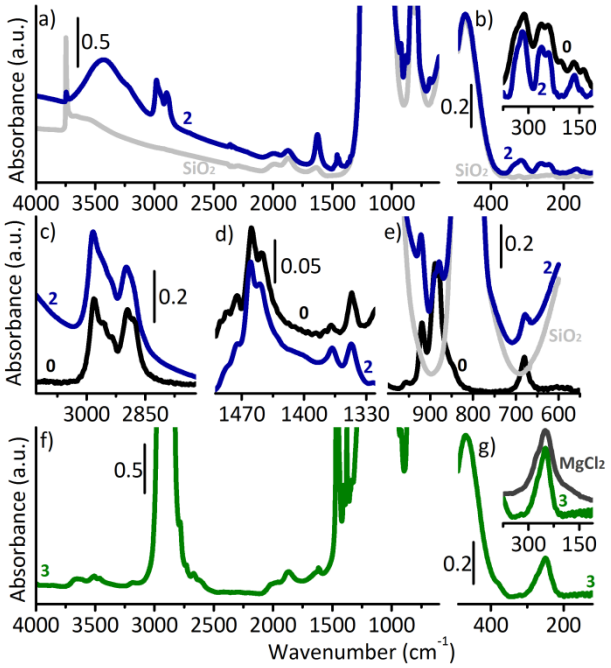

Figure 2. Parts a) and b): Mid-IR and Far-IR spectra of SiO_2/TiMg (curve 2) compared to those of bare SiO_2. A magnification of the Far-IR region is displayed in the inset of part b), where it is shown also the spectrum of the magnesium precursor (curve 0). Parts c), d) and e) show magnifications of the spectral regions where the main absorption bands characteristic of thf vibrations appear. The spectrum of the magnesium precursor is also shown for comparison (curve 0). Same color code as in parts a) and b). Parts f) and g): Mid-IR and Far-IR spectra of SiO_2/TiMg/TOAl (curve 3). A magnification of the Far-IR region is displayed in the inset of part g), where it is shown also the spectrum of crystalline $MgCl_2$.

The FT-IR spectrum of SiO_2/TiMg pre-catalyst is shown in Figure 2 (curve 2) in the whole Mid-IR (part a) and Far-IR (part b) regions, in comparison to that of dehydroxylated silica (curve SiO_2). The two spectra are dominated by the intense bands due to Si-O vibrational modes of the silica framework (1400-950 cm^{-1}) and by their overtone modes (2100-1550 cm^{-1} region).[72] The sharp absorption band observed at 3746 cm^{-1} in the spectrum of pure silica, due to isolated surface silanol groups, is almost completely consumed in the spectrum of SiO_2/TiMg. A fraction of the free silanols has been consumed because of titanium grafting, as testified by the presence, in the spectrum of SiO_2/TiMg, of two broad bands around 925 and 675 cm^{-1}, well evident in narrow frequency regions of transparency. These bands were previously assigned to perturbation of the Si-O framework modes due to titanium grafting.[59,60,62] Moreover, the consumption of the free surface silanols in the spectrum of SiO_2/TiMg is also associated to the appearance of a broad absorption band centered around 3425 cm^{-1}, which can be explained in terms of ν(OH) of ≡SiOH species hydrogen-bonded to some ligand acting as a Lewis base (either a partially uncoordinated titanium sites, or thf itself). The corresponding δ(OH) absorption band is observed around 1630 cm^{-1}. This result is different from what found for the single phase SiO_2/Ti sample, where only the grafting of the titanium precursor was observed.[47]

In addition, the spectrum of SiO_2/TiMg shows narrow absorption bands characteristic of thf vibrational modes,[73] in

the regions 3050-2800 cm^{-1} (CH_2 stretching, Figure 2c), 1500-1300 cm^{-1} (bending, wagging and twisting modes, Figure 2d), and 1100-600 cm^{-1} (C-O-C bending modes, Figure 2e). Comparison with the IR spectrum (collected in ATR mode) of the magnesium chloride tetrahydrofuranate precursor (curve 0) provides an evidence that most of the thf present in the sample is attached to magnesium sites rather than to titanium sites. Indeed, the vibrational modes of thf ligands (especially those in the 1100-600 cm^{-1} wavenumber region) are very sensitive to the Lewis acidity of the metal center to which they are bonded.[7,56] Also in the Far-IR region the spectrum of SiO_2/TiMg closely resembles that of the magnesium precursor, characterized by a complex series of absorption bands, at least partially related to Mg-Cl vibrations.

Summarizing, FT-IR spectroscopy suggests that: i) the titanium precursor is mostly grafted to the silica support through surface ≡SiOH groups, as already found for the single-phase SiO_2/Ti sample; ii) at least a fraction of the magnesium precursor remains unaltered on the silica surface (same vibrational properties), in agreement with the XRPD data (Figure 1, curve 2); iii) thf is still present in large amount, but mainly bonded to the $MgCl_x$ phase.

The IR spectrum of the SiO_2/TiMg/TOAl catalyst (curve 3 in Figure 2f) is remarkably different from that of the pre-catalyst (curve 2 in Figure 2a-e) in all the investigated wavenumber region. In particular: i) the whole spectrum is flattened (the inter-particle scattering of light decreases, because the pellet is wet); ii) the broad absorption band in the ν(OH) region completely disappears; iii) the spectrum is dominated by the intense (and out-of-scale) absorption bands due to ν(CH_x) (3000-2800 cm^{-1}) and δ(CH_x) (1500-1300 cm^{-1}) vibrational modes characteristic of TOAl and of the heptane solvent; iv) unfortunately, nothing can be said about the destiny of thf, since the corresponding absorption bands fall in wavenumber regions obscured by the previously mentioned intense bands; v) finally, in the Far-IR region (Figure 2g), the complex absorption bands due to the magnesium chloride tetrahydrofuranates phase disappear and are substituted by a well-defined band centered at 250 cm^{-1}, which is assigned to $MgCl_2$ (compare curve 3 with the spectrum of a $MgCl_2$ reference, inset in Figure 2g). Therefore, it is possible to conclude that TOAl has a profound effect on the silica-supported $MgCl_x$ phase (in agreement with XRPD data, Figure 1, curve 3), in that it removes most of the thf ligands and promotes the formation of a highly dispersed $MgCl_2$ phase, not detected by XRPD but well visible in the Far-IR spectrum.

Titanium oxidation state and local symmetry. The electronic properties of the SiO_2/TiMg pre-catalyst and the corresponding SiO_2/TiMg/TOAl catalyst were investigated by means of DR UV-Vis and Ti K-edge XANES spectroscopy. The DR UV-Vis spectra are dominated by the electronic properties of the Ti-containing phase, whereas the $MgCl_x$ phase is expected to contribute in the far UV region. Ti K-edge XANES spectroscopy is an element selective technique and as such provides information on the titanium sites only. Both techniques are sensitive to titanium oxidation state and local symmetry.[5,7,74]

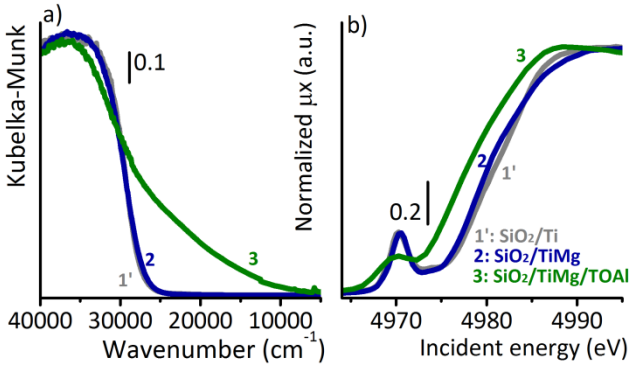

Figure 3. Diffuse Reflectance UV-Vis spectra in Kubelka-Munk units (part a) and normalized XANES spectra (part b) of SiO_2/Ti (curve 1'), SiO_2/TiMg (curve 2) and SiO_2/TiMg/TOAl (curve 3).

The DR UV-Vis and normalized XANES spectra of the pre-catalyst (curves 2 in Figure 3a and b, respectively) are very similar to those of the single phase SiO_2/Ti sample previously investigated (curves 1').[47] This observation provides a strong evidence that the titanium sites do have the same formal oxidation state (i.e. +4), and a similar coordination in the two cases (i.e. in average 6-fold coordination, where most of the chlorine ligands originally surrounding the titanium sites are substituted by oxygen ligands upon grafting on silica). Going in more details, the intense edge observed in the UV-Vis spectra around 30000 cm^{-1} is mainly due to O → Ti charge-transfer transition.[5,74,75] The pre-edge peak observed around 4970 eV in the XANES spectra is assigned to 1s → 3pd transitions.[5,47,75] The low intensity of this peak (about 0.2 in normalized absorption) is indicative of a high coordination, in agreement with UV-Vis data. Both pre-edge and edge regions are quite broad, indicating a large heterogeneity of titanium sites.

Addition of TOAl causes significant changes in both DR UV-Vis and XANES spectra, which testify a reduction of the titanium sites. In particular, in the UV-Vis spectrum a broad and unstructured absorption appears in the visible region, where d-d transitions characteristic of Ti^{3+} sites in a 6-fold coordination are expected to occur.[76] Simultaneously, the intense edge in the charge-transfer region becomes broader and shifts at higher wavenumber values. In the XANES spectra, the absorption edge shifts towards lower energy (from 4979 to 4977 eV, as evaluated at the maximum of the derivative spectra), as expected for reduction of Ti^{4+} to Ti^{3+}; simultaneously, the pre-edge peak decreases in intensity, becomes broader and slightly shifts at lower energy. In summary, both UV-Vis and XANES spectra demonstrate that TOAl reduces the Ti^{4+} sites originally grafted at the SiO_2 surface to a large variety of Ti^{3+} sites, as expected on the basis of the specialized literature.[1-2]

Local structure around titanium sites and ligands identification. The broad character of both DR UV-Vis and Ti K-edge XANES spectra does not allow to extract precise information on the nature of the titanium phase in both pre-catalyst and catalyst. For this reason, we turned our attention to two element selective spectroscopic techniques (EXAFS and vtc-XES), whose potential in characterizing the type of ligands and the local structure of transition metals on inorganic matrices was largely demonstrated in the past.[5,11,44]

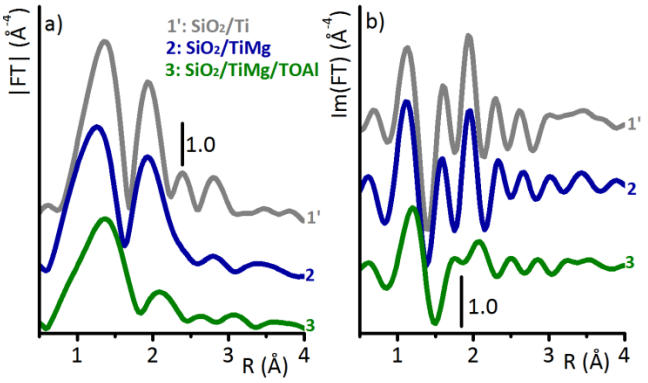

Figure 4. Phase-uncorrected Fourier-Transform (in both modulus and imaginary parts, parts a and b, respectively) of the k^3-weighted $\chi(k)$ EXAFS function for SiO_2/Ti (curve 1'), SiO_2/TiMg (curve 2) and SiO_2/TiMg/TOAl (curve 3). The spectra were extracted in the Δk = 2.0 – 10.0 $Å^{-1}$ range, and vertically translated for clarity.

The phase-uncorrected Fourier Transform (FT) of the $k^3\chi(k)$ EXAFS function for the SiO_2/TiMg pre-catalyst is shown in Figure 4 (curve 2) in both modulus and imaginary parts (parts a and b, respectively), in comparison with that of the single-phase SiO_2/Ti sample (curve 1') that was discussed in our previous work.[47] Both spectra are dominated by two main contributions, centered around 1.4 and 2.0 Å, respectively (values not phase-corrected), which were assigned to the co-presence of oxygen and chlorine ligands around the titanium site. The similarity of the two spectra provides an evidence that the local structure around the titanium sites is comparable in the two samples, in agreement with DR UV-Vis and XANES data. Hence, the presence of the $MgCl_x$ phase seems to have a minor effect in influencing the local structure of the titanium sites in the pre-catalyst, which are prevalently grafted to the silica surface through Ti-O bonds.

The FT of the EXAFS spectrum for the catalyst obtained after the interaction of the pre-catalyst with TOAl is substantially different, testifying that some changes occurred in the local structure of the titanium sites. In particular, the spectrum of the catalyst is less intense than that of the pre-catalyst and is dominated by a first shell signal centered around 1.4 Å (with a shoulder around 1.0 Å), whereas the signal at the longer distance characteristic of chlorine ligands is almost disappeared (particularly evident in the imaginary part). Hence, from a qualitative analysis of the EXAFS spectrum, it might be suggested that upon interaction of the pre-catalyst with TOAl most of the titanium sites remain attached to the silica surface and the few chlorine ligands originally present are removed. However, the data discussed above demonstrated that activation by TOAl promotes the formation of a highly dispersed $MgCl_2$ phase. In presence of such an important structural rearrangement, it must be taken into account the possibility that the titanium phase may be detached from the silica surface and may interact with $MgCl_2$, mimicking what happens for heterogeneous $MgCl_2$-based Ziegler-Natta catalysts.

Unfortunately, a quantitative analysis of the EXAFS spectra was heavily affected by problems intrinsic to the nature of the analyzed sample, and possibly common to other systems. The main problem is related to the presence in the titanium coordination sphere of several ligands at similar coordination distances, whose contribution is at least partially out-of-phase.

Table 2. Optimized parameters in the analysis of the EXAFS spectrum for the SiO_2/TiMg/TOAl according to three different structural models of increasing complexity. $N_{ind} = 2\Delta k\Delta R/\pi > 10$.

Variables	FIT 1 [a]	FIT 2 [b]	FIT 3 [c]
ΔE (eV)	-6 ± 3	-4 ± 3	-4 ± 2
N_O	3.2 ± 1.0	3.3 ± 0.9	1.1 ± 0.5
R_O (Å)	1.90 ± 0.03	1.92 ± 0.02	1.84 ± 0.02
σ_O^2 ($Å^2$)	0.019 ± 0.006	0.019 ± 0.006	0.007 ± 0.005
N_{Clt}			1.8 ± 0.6
R_{Clt} (Å)			2.18 ± 0.03
σ_{Clt}^2 ($Å^2$)			0.013 ± 0.003
N_{Clb}		0.3 ± 0.4	1.8 ±0.6
R_{Clb} (Å)		2.46 ± 0.03	2.43 ± 0.03
σ_{Clb}^2 ($Å^2$)		0.005 ± 0.014	0.013 ± 0.003
R_{factor}	0.06	0.02	0.01

[a] FIT 1 was performed by considering the contribution of only oxygen ligands; [b] FIT 2 considered the presence of two type of ligands: oxygen and chlorine (Cl_b = bridged chlorine); [c] FIT 3 was done by adding to the model used in FIT 2 the contribution from a second type of chlorine ligand (Cl_t = terminal chlorine), at shorter distance.

This means that any quantitative evaluation of the titanium coordination numbers is simply not meaningful and, at most, only coordination distances can be determined. An example of the problems encountered in the data analysis is discussed below for the SiO_2/TiMg/TOAl catalyst. Different strategies were followed to fit the experimental spectrum, as summarized in Table 2. Figure 5 shows the best fits overlapped to the experimental data, and the separate contributions of different ligands to the fits.

A first fit (FIT 1 in Table 2 and Figure 5a and b) was attempted by including the contribution of oxygen only. The fit was performed by optimizing the following parameters: i) ΔE_0; ii) the coordination number (N_O), that was re-normalized to the S_0^2 value obtained by fitting the signal of TiO_2 reference compound; iii) the Ti-O distance; iv) the Debye-Waller factor (σ_O^2). The results are summarized in Table 2: in average, each titanium atom is surrounded by 3.2 ± 1.0 oxygen ligands at a distance of R_O = 1.90 ± 0.03 Å, with a quite large Debye-Waller factor (σ_O^2 = 0.019 ± 0.006 $Å^2$). Although the coordination distance looks reasonable, the number of ligands is clearly underestimated. The fit is obviously unable to reproduce the experimental signal in the 2.0-3.0 Å region, which is due to at least one additional coordination shell overlooked in the model of FIT 1. This problem is considered in FIT 2. However, the results do not greatly change by considering the co-presence of oxygen and chlorine ligands (Cl_b = bridged chlorine), that may be present if the titanium-containing phase interacts with the highly dispersed $MgCl_2$ phase. FIT 2 (Figure 5d) was performed by optimizing the following parameters: i) a single ΔE_0, common to the two scattering paths; ii) the coordination numbers for both ligands (N_O and N_{Clb}), re-normalized to the S_0^2 values obtained by fitting the signals of TiO_2 and α-$TiCl_3$ reference compounds; iii) the two Ti-L distance (L = ligand); iv) the two Debye-Waller factors for the two ligands. According to the fit, in average each titanium atom has only 3.6 ligands, which is incompatible with the other available experimental data.

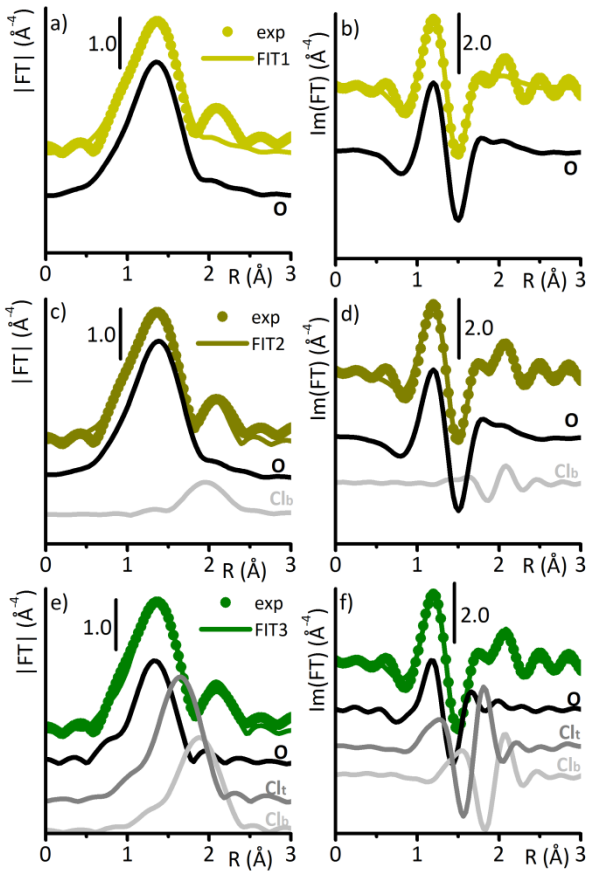

Figure 5. Analysis of the EXAFS spectrum for the SiO_2/TiMg/TOAl catalyst. Parts a) and b) refer to FIT 1, which includes the contribution of only oxygen ligands. The experimental phase-uncorrected FT of the $k^3\chi(k)$ EXAFS function is shown in both modulus and imaginary parts (dotted curves in parts a and b, respectively), overlapped to the result of the fit (full lines). The contributions of the oxygen ligands is also shown, vertically translated for clarity. Parts c) and d) are the same for FIT 2, which includes the contributions of oxygen and chlorine (Cl_b) ligands. Parts e) and f) are the same for FIT 3, which includes an additional chlorine ligand at shorter distance (Cl_t). The results of the three fits are summarized in Table 2.

A third fit (FIT 3 in Table 2 and Figure 5e and f) was then performed by considering, in addition to the two ligands used in FIT 2 the presence of a second type of chlorine ligands (Cl_t = terminal chlorine) at a distance shorter than Cl_b. It is worth noticing that the co-presence of terminal and bridged chlorine ligands (at shorter and longer distances, respectively) in the titanium coordination sphere was recently reported by some of us for analogous Ziegler-Natta catalysts not silica-supported.[8] The agreement with the experimental data is better than FIT 2 (R_{factor} in Table 2). In this case the coordination numbers are completely reversed: 1.1 ± 0.5 oxygen ligands at a distance of R_O = 1.84 ± 0.02 Å (with σ_O^2 = 0.007 ± 0.005 Å^2), 1.8 ± 0.6 chlorine ligands at a distance of R_{Clt} = 2.18 ± 0.03 Å, and 1.8 ± 0.6 chlorine ligands at a distance of R_{Clb} = 2.43 ± 0.03 Å (with σ_{Cl}^2 = 0.013 ± 0.003 Å^2). The results of this fit are more realistic. In average, each titanium site has about 5 ligands, which is compatible with previously discussed results and also with some of the widely accepted models for titanium active sites in $MgCl_2$-supported Ziegler-Natta catalysts. It is important to observe that the Debye-Waller factors for the chlorine ligands are quite large, accounting for a large heterogeneity of species.

We might speculate on the presence of one available coordination vacancy around the titanium sites, which would be predictable on the basis of the models proposed for titanium sites in classical ($MgCl_2$-supported) Ziegler-Natta catalysts. We might also hazard the hypothesis that the low-Z element detected by EXAFS is not an oxygen ligand, but rather a carbon ligand (EXAFS is unable to distinguish among oxygen and carbon ligands), as expected by assuming the Cosse-Arlman mechanism for active sites formation.[77] Nevertheless, it is common opinion that the catalytically active titanium sites are only a few of the total. Hence, it looks more safe to interpret the EXAFS results in terms of co-presence of two different phases: a minor fraction of isolated titanium sites still grafted to silica, and a $TiCl_x$ phase where different titanium sites are bridged through chlorine ligands to a highly dispersed, silica-supported, $MgCl_2$ phase. The active titanium sites bearing an alkyl ligand, if present, may be easily hidden by these two phases.

Opposite to EXAFS, vtc-XES spectroscopy does not suffer of interference problems and it is a valuable technique for ligand identification.[78-80] The vtc-XES spectrum of SiO_2/TiMg pre-catalyst is compared in Figure 6 to that of the single phase SiO_2/Ti sample, discussed in our previous work;[47] the assignment of the Kβ" and $K\beta_{2,5}$ fluorescence lines is also reported. It is useful to recall that Kβ" fluorescence lines are due to transitions involving mainly molecular orbitals with ligand s-atomic character, and thus they are useful for ligand identification; whereas $K\beta_{2,5}$ fluorescence lines are due to transitions involving primarily molecular orbitals having a ligand p-atomic character, and hence they are sensitive to the valence orbitals.

The vtc-XES spectrum of SiO_2/TiMg (curve 2) is very similar to that of SiO_2/Ti (curve 1'), confirming once more that the local structure and the electronic state of the titanium sites is similar in the two samples. Also in the SiO_2/TiMg pre-catalyst the titanium sites are grafted to silica through some oxygen ligands (identified by the intense Kβ" line centered at 4947 eV), and retain in the coordination sphere a few chlorine ligands (identified by the Kβ" line at 4954 eV) and a few thf

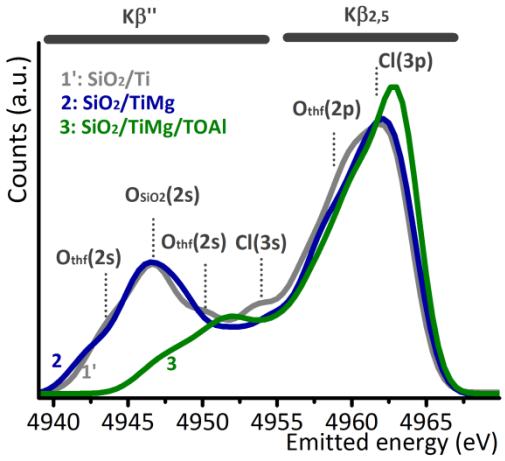

Figure 6. Normalized vtc-XES spectra of SiO_2/Ti (curve 1'), SiO_2/TiMg (curve 2) and SiO_2/TiMg/TOAl (curve 3). The Kβ" and $K\beta_{2,5}$ regions are indicated on the top, and the main features identifying oxygen and chlorine ligands are labeled.

ligands (Kβ" lines at 4943 and 4950 eV). However, a better comparison allows to observe that the Kβ" lines assigned to transition involving mainly molecular orbitals lying on thf ligands are shifted at lower energy in the spectrum of the pre-catalyst. Although the increased complexity of the system makes a systematic investigation (as presented in our previous work)[47] not feasible, preliminary DFT calculations[81] proved that the shift of the Kβ" lines assigned to thf ligands can be reproduced by considering open thf ligands. This means that the presence of the magnesium phase on the silica surface adjacent to the grafted titanium sites has an influence on the stability of the thf ligands. It is interesting to observe that experimental evidences, supported by DFT calculations, for opening of thf with consequent formation of titanium alkoxy surface species have been provided recently for a similar $MgCl_2$/thf/$TiCl_4$ system.[29]

The vtc-XES spectrum of the SiO_2/TiMg/TOAl catalyst is substantially different from that of the pre-catalyst, demonstrating that the activator drastically affects the local structure of the titanium sites, in agreement with EXAFS data. In particular, in the Kβ" region:

i) the lines identifying the thf ligand are no more present, providing evidence that most of the thf (also the opened one) has been displaced by TOAl from the titanium sites, in good agreement with previous literature about activation of commercial silica-supported Ziegler-Natta catalysts containing thf or other electron donors;[1-2]

ii) the band at 4947 eV characteristic of oxygen belonging to silica is much less intense, suggesting that most of the titanium sites are no more grafted to silica. This evidence agrees with the low coordination number of the Ti-O shell found in FIT 3 of the EXAFS data (see Table 1);

iii) a new and well visible band appears around 4952 eV. A similar band was recently observed by some of us in the vtc-XES spectrum of a similar, not silica-supported TiMg/TOAl catalyst, although much less intense.[8] The energy position of this band is compatible both with carbon ligands (that might be present according to the Cossee-Arlman mechanism for active sites formation[77]) and with bridged-chlorine ligands, whose presence is supported by the data discussed above.

In the $K\beta_{2,5}$ region, the line assigned to thf ligand disappears, whereas the band characteristic of chlorine ligands increases in intensity and becomes sharper, in close similarity to the spectrum of violet $TiCl_3$ reference compound.[8]

Summarizing, the whole set of EXAFS and vtc-XES data provide evidence that the local structure around the titanium sites is totally reconstructed after the interaction of the pre-catalyst with TOAl. A consistent fraction of titanium sites has chlorine ligands in the first coordination sphere, testifying that they are mainly detached from the silica surface and interact with a highly dispersed $MgCl_2$ phase, whose presence was clearly revealed by Far-IR spectroscopy. According to EXAFS data analysis, two types of chlorine ligands are present: terminal chlorine species at shorter distance (2.18 ± 0.03 Å), and bridged chlorine species at longer distance (2.43 ± 0.03 Å). Vtc-XES data might be compatible with the presence of a few titanium sites bearing an alkyl ligand, but definitive proofs are still missing.

3.2 In situ ethylene polymerization. Finally, we tested the SiO_2/TiMg/TOAl catalyst in ethylene polymerization. The catalytic performances of this commercial catalyst are reported in the specialized literature for gas-phase ethylene polymerization conducted in a fluidized-bed reactor.[32-38] However, it is of paramount importance to verify that the activation conditions adopted during the spectroscopic investigation of the SiO_2/TiMg/TOAl system lead to a catalyst active in ethylene polymerization. To this aim, we monitored ethylene polymerization at room temperature by in situ FT-IR spectroscopy, following the same approach extensively used to investigate the initial steps of ethylene polymerization on the Phillips catalyst.[5,44-46,82-85] The presence of the aluminum alkyl activator and of the solvent prevented up to now the exploitation of the same method to follow in situ olefin polymerization on industrially relevant Ziegler-Natta catalysts. To the best of our knowledge, the only FT-IR spectra showing in situ ethylene polymerization on Ziegler-Natta catalysts were collected in Attenuated Total Reflection (ATR) mode on a planar model of Ziegler-Natta catalyst.[25]

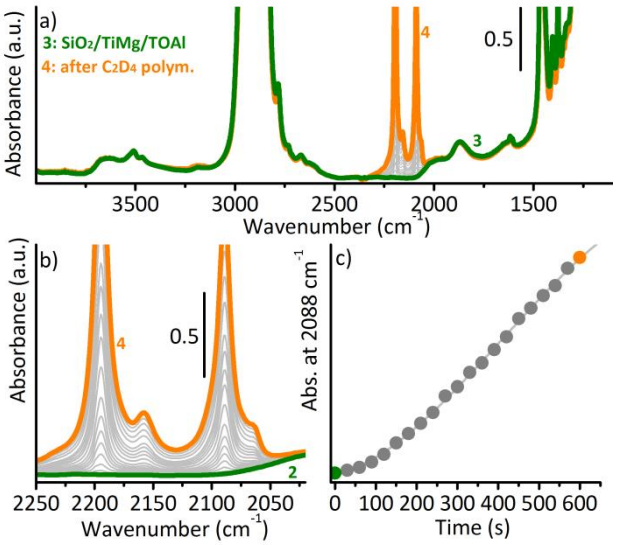

Figure 7. Part a) FT-IR spectra collected during polymerization of C_2D_4 (room temperature, P_{C2D4} = 100 mbar) on the SiO_2/TiMg/TOAl catalyst. Curve 3: spectrum of the catalyst before interaction with C_2D_4; curve 4: after 10 minutes of C_2D_4 polymerization. Gray spectra were collected at regular time interval during polymerization. Part b) shows an enlargement of the spectral region where the absorption bands characteristic of dPE appear. Part c) reports the intensity of the absorption band at 2088 cm^{-1} as a function of time.

We found that a thin pellet of the SiO_2/TiMg/TOAl catalyst, obtained upon impregnation of a thin pellet of the SiO_2/TiMg pre-catalysts with the TOAl/heptane solution (following exactly the same procedure used during the previous spectroscopic investigations, approximate Al/Ti ratio of 10), is measurable by FT-IR spectroscopy in transmission (Figure 2f), although most of the spectral regions were obscured by the intense and out-of-scale absorption bands due to TOAl, to the solvent and to the reaction by-products (e.g. $Al(Oct)_2Cl$). In our prospect, the presence of liquid TOAl/heptane in the silica pores may simulate, if not industrially significant polymerization conditions, at least pre-polymerization conditions (where the monomer is fed onto the catalyst in presence of the activator and of the solvent at low pressure and low temperature), simultaneously allowing to perform in situ FT-IR experiments in transmission mode. In order to separate

the vibrational manifestation of the polymer from those of the activator, we worked with deuterated ethylene (d-ethylene). As anticipated in the Experimental section, the experimental procedure is crucial. In particular, a partial removal of the solvent (upon degassing the reaction cell) was found to have a negative effect, probably enhancing the catalyst deactivation. On the contrary, in the presence of the solvent ethylene polymerization readily takes place, already at low ethylene pressure and at room temperature.

A typical experiment is shown in Figure 7a in the whole frequency range, whereas Figure 7b shows an enlargement of the spectral region characteristic of d-polyethylene. Upon d-ethylene admission in the reaction cell (room temperature, P_{C2D4} = 100 mbar), two intense absorption bands gradually grow at 2195 and 2089 cm^{-1}, which are assigned to $\nu_{asym}(CD_2)$ and $\nu_{sym}(CD_2)$ vibrational modes of the d-polyethylene chains. Other two weaker bands are observed at 2158 and 2065 cm^{-1}, which are assigned to the $2\delta(CD_2)$ mode (fundamental vibration around 1085 cm^{-1}) and to the combination of $\delta(CD_2)+2\rho(CD_2)$ (fundamental $\rho(CD_2)$ mode around 520 cm^{-1}). Figure 7c shows a plot of the intensity of the IR band at 2088 cm^{-1} (chosen here as a reference band to monitor the polymer growth) versus time. After a short induction period (about 1 minute), which is likely due to the diffusion of the monomer into the liquid TOAl/heptane phase, an almost linear dependence is observed within the investigated time interval, and no evidence of catalyst deactivation was observed. It is worth of notice that these data do not have the intention to give any quantitative information on the kinetics of the reaction, but rather to demonstrate that it is possible to look at a silica-supported Ziegler-Natta catalyst in action by means of spectroscopic techniques. This is not a trivial job for most of the heterogeneous catalysts, and it has been precluded so far for Ziegler-Natta catalysts.

4. CONCLUSIONS

The structural, vibrational and electronic properties of an industrially relevant, silica-supported, Ziegler-Natta catalyst were investigated by a large arsenal of characterization techniques during all the steps of catalyst preparation, including pre-catalyst activation and ethylene polymerization. It was demonstrated that the alkyl-aluminum activator significantly reconstruct the whole pre-catalyst, acting on all the catalyst constituents and not only on the $TiCl_x$ phase. In particular, it was found that TOAl removes most of the thf originally present in the pre-catalyst and promotes the formation of a $MgCl_2$ phase highly dispersed on the silica surface, not detected by XRD but identified by means of Far-IR spectroscopy. Simultaneously, the titanium sites get reduced. Although we cannot be fully quantitative on the amount of titanium sites which are reduced by TOAl, the profound modifications observed with all the employed techniques do suggest that the reduction process involves most of the titanium sites in the pre-catalyst. Most of them detach from the silica surface to form $TiCl_x$ species connected to the silica-supported $MgCl_2$ phase through bridging chlorine ligands, and characterized by the presence of terminal chlorine ligands at shorter distances. Hence, the final catalytic phase would resemble that formed in absence of silica, although probably much more dispersed.

Although at present we cannot distinguish between active and spectator sites, the herein reported data are among the few experimental evidences on the structure of the titanium sites at a molecular scale in industrially significant silica-supported Ziegler-Natta catalysts. Finally, and very important, the same catalyst was observed by means of FT-IR spectroscopy during ethylene polymerization in co-presence of the activator, the solvent and the monomer. These results definitely validate the step-by-step synthetic approach used in this work, and open interesting perspectives in the field of in situ investigation of Ziegler-Natta catalysts in action in industrially significant polymerization conditions. We believe that a systematic investigation of all the catalyst's components by means of a multi-technique approach (as proposed in this work) might be the first fundamental step towards the understanding of their mutual interactions and functions, down to a level of detail rarely reached by other methods, making the design of these catalysts a realistic ambition for the future.

AUTHOR INFORMATION

Corresponding Author

* E-mail: elena.groppo@unito.it

Funding Sources

C.L. thanks the Mega-grant of the Russian Federation Government to support scientific research at the Southern Federal University, No.14.Y26.31.0001.

ACKNOWLEDGMENT

We are grateful to Wim Bras (BM26 at ESRF), Roelof van Silfhout and Anton Kachatkou (The University of Manchester) for the fruitful collaboration during the XAS measurements and Pieter Glatzel, Mauro Rovezzi and Christophe Lapras (ID26 at ESRF) for the help during the XES experiments. We are indebted with Harald Muller (Chemical Lab at ESRF) for providing us the indispensable and always perfect glove-box during the experiments at ESRF. We would like to thank Francesco Masi for the valuable discussion from an industrial perspective and Prof. Adriano Zecchina for the everyday dialog and constant encouragement.

ABBREVIATIONS

thf, tetrahydrofuran; TOAl, trioctyl-aluminum.

REFERENCES

(1) Albizzati, E.; Giannini, U.; Collina, G.; Noristi, L.; Resconi, L., *Catalysts and polymerizations*, in: Polypropylene Handbook; Moore, E. P. J., Ed.; Hanser-Gardner Publications: Cincinnati, OH, **1996**.

(2) Busico, V., *MRS Bulletin* **2013**, *38*, 224-228.

(3) Klapper, M.; Joe, D.; Nietzel, S.; Krumpfer, J. W.; Müllen, K., *Chem. Mater.* **2014**, *26*, 802-819.

(4) Busico, V., *Dalton Trans.* **2009** 8794-8802.

(5) Groppo, E.; Seenivasan, K.; Barzan, C., *Catal. Sci. Technol.* **2013**, *3*, 858-878.

(6) Dwivedi, S.; Taniike, T.; Terano, M., *Macromol. Chem. Phys.* **2014**, *215*, 1698-1706.

(7) Seenivasan, K.; Sommazzi, A.; Bonino, F.; Bordiga, S.; Groppo, E., *Chem. Eur. J* **2011**, *17*, 8648-8656.

(8) Groppo, E.; Gallo, E.; Seenivasan, K.; Lomachenko, K. A.; Sommazzi, A.; Bordiga, S.; Glatzel, P.; Van Silfhout, R.; Kachatkou, A.; Bras, W.; Lamberti, C., *Chemcatchem* **2015**, *7*, 1432-1437.

(9) Lamberti, C.; Groppo, E.; Spoto, G.; Bordiga, S.; Zecchina, A., *Adv. Catal.* **2007**, *51*, 1-74.

(10) Lamberti, C.; Zecchina, A.; Groppo, E.; Bordiga, S., *Chem. Soc. Rev.* **2010**, *39*, 4951–5001.

(11) Bordiga, S.; Groppo, E.; Agostini, G.; Van Bokhoven, J. A.; Lamberti, C., *Chem. Rev.* **2013**, *113*, 1736−1850.
(12) Frenkel, A. I.; Rodriguez, J. A.; Chen, J. G., *ACS Catal.* **2012**, *2*, 2269-2280.
(13) Lysova, A. A.; Koptyug, I. V., *Chem. Soc. Rev.* **2010**, *39*, 4585-4601.
(14) Schoonheydt, R. A., *Chem. Soc. Rev.* **2010**, *39*, 5051-5066.
(15) Tromp, M., *Philos. Trans. R. Soc. A Math. Phys. Eng. Sci.* **2015**, *373*, Article number 20130152.
(16) Vimont, A.; Thibault-Starzyk, F.; Daturi, M., *Chem. Soc. Rev.* **2010**, *39*, 4928-4950.
(17) Wachs, I. E.; Roberts, C. A., *Chem. Soc. Rev.* **2010**, *39*, 5002-5017.
(18) Zaera, F., *Chem. Soc. Rev.* **2014**, *43*, 7624-7663.
(19) van Bokhoven, J. A.; Lamberti, C., *X-ray absorption and emission spectroscopy for catalysis*, in: X-Ray Absorption and X-ray Emission Spectroscopy: Theory and Applications; van Bokhoven, J. A.; Lamberti, C., Ed.; John Wiley & Sons, **2015**; Vol. 2.
(20) McKenna, T. F. L.; Tioni, E.; Ranieri, M. M.; Alizadeh, A.; Boisson, C.; Monteil, V., *Can. J. Chem. Eng.* **2013**, *91*, 669-686.
(21) Oleshko, V. P.; Crozier, P. A.; Cantrell, R. D.; Westwood, A. D., *Macromol. Rapid Commun.* **2001**, *22*, 34-40.
(22) Andoni, A.; Chadwick, J. C.; Niemantsverdriet, H. J. W.; Thune, P. C., *Macromol. Rapid Commun.* **2007**, *28*, 1466-1471.
(23) Andoni, A.; Chadwick, J. C.; Milani, S.; Niemantsverdriet, H.; Thune, P. C., *J. Catal.* **2007**, *247*, 129-136.
(24) Andoni, A.; Chadwick, J. C.; Niemantsverdriet, H. J. W.; Thune, P. C., *J. Catal.* **2008**, *257*, 81-86.
(25) Andoni, A.; Chadwick, J. C.; Niemantsverdriet, J. W.; Thune, P. C., *Catal. Lett.* **2009**, *130*, 278-285.
(26) Morra, E.; Giamello, E.; Van Doorslaer, S.; Antinucci, G.; D'Amore, M.; Busico, V.; Chiesa, M., *Angew. Chem. Int. Ed.* **2015**, *54*, 4857-4860.
(27) Giannini, U.; Albizzati, E.; Parodi, S.; Pirinoli, F., Catalysts for polymerizing olefins. US Patent 4,124,532, November 7, 1978.
(28) Sobota, P.; Utko, J.; Lis, T., *J. Chem. Soc. Dalton Trans.* **1984** 2077-2079.
(29) Grau, E.; Lesage, A.; Norsic, S.; Copéret, C.; Monteil, V.; Sautet, P., *ACS Catal.* **2013**, *3*, 52-56.
(30) Pirinen, S.; Koshevoy, I. O.; Denifl, P.; Pakkanen, T. T., *Organometallics* **2013**, *32*, 4208-4213.
(31) Pirinen, S.; Jayaratne, K.; Denifl, P.; Pakkanen, T. T., *J. Mol. Catal. A Chem.* **2014**, *395*, 434-439.
(32) Goeke, G. L.; Wagner, B. E.; Karol, F. J., Impregnated polymerization catalyst, process for preparing and use for ethylene copolymerization. US Patent 4,302,565, 1981.
(33) Karol, F. J.; Goeke, G. L.; Wagner, B. E.; Fraser, W. A.; Jorgersen, R. J.; Friis, N., Preparation of ethylene copolymers in fluid bed reactors. U.S. Patent 4,302,566, 1981.
(34) Karol, F. J., *Catal. Rev. Sci. Eng.* **1984**, *26*, 557.
(35) Karol, F. J.; Cann, K. J.; Wagner, B. E., in: Transition Metals and Organometallics as Catalysts for Olefin Polymerization; Kaminsky, W.; Sinn, H., Ed.; Springer: Berlin, Germany, **1988**, p. 149.
(36) Kissin, Y. V., in: Alkene Polymerization Reactions with Transition Metal Catalysts; Elsevier: Amsterdam, The Netherlands, **2008**.
(37) Nowlin, T. E.; Mink, R. I.; Kissin, Y. V., in: Transition Metal Polymerization Catalysts; Hoff, R.; Mathers, R. T., Ed.; John Wiley & Sons: Hoboken, USA., **2009**.
(38) Nowlin, T. E., *Business and Technology of the Global Polyethylene Industry*, in; Scrivener Publishing LLC: New York, **2014**.
(39) Pullukat, T. J.; Hoff, R. E., *Catal. Rev.-Sci. Eng.* **1999**, *41*, 389-428.
(40) Severn, J. R.; Chadwick, J. C.; Duchateau, R.; Friederichs, N., *Chem. Rev.* **2005**, *105*, 4073-4147.
(41) McKenna, T. F. L.; Di Martino, A.; Weickert, G.; Soares, J. B. P., *Macromol. React. Eng.* **2010**, *4*, 40-64.
(42) Lee, M. Y.; Scott, S. L., *Chem.-Eur. J.* **2011**, *17*, 4632-4639.
(43) Campos, J. M.; Lourenço, J. P.; Cramail, H.; Ribeiro, M. R., *Prog. Polym. Sci.* **2012**, *37*, 1764-1804.
(44) Groppo, E.; Lamberti, C.; Bordiga, S.; Spoto, G.; Zecchina, A., *Chem. Rev.* **2005**, *105*, 115-183.
(45) Groppo, E.; Lamberti, C.; Spoto, G.; Bordiga, S.; Magnacca, G.; Zecchina, A., *J. Catal.* **2005**, *236*, 233-244.
(46) Zecchina, A.; Groppo, E., *Proc. R. Soc. A-Math. Phys. Eng. Sci.* **2012**, *468*, 2087-2098.
(47) Seenivasan, K.; Gallo, E.; Piovano, A.; Vitillo, J. G.; Sommazzi, A.; Bordiga, S.; Lamberti, C.; Glatzel, P.; Groppo, E., *Dalton Trans.* **2013**, *42*, 12706-12713.
(48) Manxzer, L. E., *Inorg. Synth.* **1982**, *21*, 135-136.
(49) Nikitenko, S.; Beale, A. M.; van der Eerden, A. M. J.; Jacques, S. D. M.; Leynaud, O.; O'Brien, M. G.; Detollenaere, D.; Kaptein, R.; Weckhuysen, B. M.; Bras, W., *J. Synchrot. Radiat.* **2008**, *15*, 632-640.
(50) van Silfhout, R.; Kachatkou, A.; Groppo, E.; Lamberti, C.; Bras, W., *J. Synchrotron Radiat.* **2014**, *21*, 401–408.
(51) Ravel, B.; Newville, M., *J. Synchrot. Radiat.* **2005**, *12*, 537-541.
(52) Zabinsky, S. I.; Rehr, J. J.; Ankudinov, A. L.; Albers, R. C.; Eller, M. J., *Phys. Rev. B* **1995**, *52*, 2995.
(53) Gallo, E.; Lamberti, C.; Glatzel, P., *Phys. Chem. Chem. Phys.* **2011**, *13*, 19409-19419.
(54) Gallo, E.; Bonino, F.; Swarbrick, J. C.; Petrenko, T.; Piovano, A.; Bordiga, S.; Gianolio, D.; Groppo, E.; Neese, F.; Lamberti, C.; Glatzel, P., *ChemPhysChem* **2013**, *14*, 79-83.
(55) Neese, F., *Wiley Interdiscip. Rev.-Comput. Mol. Sci.* **2012**, *2*, 73-78.
(56) Kim, I.; Chung, M. C.; Choi, H. K.; Kim, J. H.; Woo, S. I., *Stud. Surf. Sci. Catal.* **1990**, *56*, 323-343.
(57) Kim, J. H.; Jeong, Y. T.; Woo, S. I., *J. Polym. Sci. A* **1994**, *32*, 2979-2987.
(58) Morrow, B. A.; Hardin, A. H., *J. Phys. Chem.* **1979**, *83*, 3135-3141.
(59) Kinney, J. B.; Staley, R. H., *J. Phys. Chem.* **1983**, *87*, 3735-3740.
(60) Haukka, S.; Lakomaa, E. L.; Jylha, O.; Vilhunen, J.; Hornytzkyj, S., *Langmuir* **1993**, *9*, 3497-3506.
(61) Haukka, S.; Lakomaa, E. L.; Root, A., *J. Phys. Chem.* **1993**, *97*, 5085-5094.
(62) Kytokivi, A.; Haukka, S., *J. Phys. Chem. B* **1997**, *101*, 10365-10372.
(63) Schrijnemakers, K.; Van Der Voort, P.; Vansant, E. F., *Phys. Chem. Chem. Phys.* **1999**, *1*, 2569-2572.
(64) Basset, J. M.; Lefebvre, F.; Santini, C., *Coord. Chem. Rev.* **1998**, *180*, 1703-1723.
(65) Coperet, C.; Chabanas, M.; Saint-Arroman, R. P.; Basset, J. M., *Angew. Chem.-Int. Edit.* **2003**, *42*, 156-181 and references therein.
(66) Rascon, F.; Wischert, R.; Coperet, C., *Chem. Sci.* **2011**, *2*, 1449-1456.
(67) Gajan, D.; Coperet, C., *New J. Chem.* **2011**, *35*, 2403-2408.
(68) Bini, F.; Rosier, C.; Saint-Arroman, R. P.; Neumann, E.; Dablemont, C.; de Mallmann, A.; Lefebvre, F.; Niccolai, G. P.; Basset, J. M.; Crocker, M.; Buijink, J. K., *Organometallics* **2006**, *25*, 3743-3760.
(69) Tosin, G.; Santini, C. C.; Taoufik, M.; De Mallmann, A.; Basset, J. M., *Organometallics* **2006**, *25*, 3324-3335.
(70) Saint-Arroman, R. P.; Basset, J. M.; Lefebvre, F.; Didillon, B., *Appl. Catal. A-Gen.* **2005**, *290*, 181-190.
(71) Le Roux, E.; Chabanas, M.; Baudouin, A.; de Mallmann, A.; Coperet, C.; Quadrelli, E. A.; Thivolle-Cazat, J.; Basset, J. M.; Lukens, W.; Lesage, A.; Emsley, L.; Sunley, G. J., *J. Am. Chem. Soc.* **2004**, *126*, 13391-13399.
(72) Ricchiardi, G.; Damin, A.; Bordiga, S.; Lamberti, C.; Spano, G.; Rivetti, F.; Zecchina, A., *J. Am. Chem. Soc.* **2001**, *123*, 11409-11419.
(73) Cadioli, B.; Gallinella, E.; Coulombeau, C.; Jobic, H.; Berthier, G., *J. Phys. Chem.* **1993**, *97*, 7844-7856.
(74) Bordiga, S.; Coluccia, S.; Lamberti, C.; Marchese, L.; Zecchina, A.; Boscherini, F.; Buffa, F.; Genoni, F.; Leofanti, G.; Petrini, G.; Vlaic, G., *J. Phys. Chem.* **1994**, *98*, 4125-4132.

(75) Bordiga, S.; Bonino, F.; Damin, A.; Lamberti, C., *Phys. Chem. Chem. Phys.* **2007**, *9*, 4854-4878.
(76) Figgis, B. N., *Introduction to ligand fields*; John Wiley & Sons: New York, **1966**.
(77) Cossee, P., *J. Catal.* **1964**, *3*, 80-88.
(78) Glatzel, P.; Bergmann, U., *Coord. Chem. Rev.* **2005**, *249*, 65-95.
(79) Glatzel, P.; Weng, T.-C.; Kvashnina, K.; Swarbrick, J.; Sikora, M.; Gallo, E.; Smolentsev, N.; Mori, R. A., *J. Electron Spectrosc. Relat. Phenom.* **2013**, *188*, 17–25.
(80) Singh, J.; Lamberti, C.; van Bokhoven, J. A., *Chem. Soc. Rev.* **2010**, *39*, 4754-4766.
(81) Gallo, E., **2013**.
(82) Groppo, E.; Lamberti, C.; Bordiga, S.; Spoto, G.; Zecchina, A., *J. Catal.* **2006**, *240*, 172-181.
(83) Groppo, E.; Estephane, J.; Lamberti, C.; Spoto, G.; Zecchina, A., *Catal. Today* **2007**, *126*, 228-234.
(84) Groppo, E.; Damin, A.; Otero Arean, C.; Zecchina, A., *Chem. Eur. J.* **2011**, *17*, 11110 – 11114.
(85) Barzan, C.; Groppo, E.; Quadrelli, E. A.; Monteil, V.; Bordiga, S., *Phys.Chem.Chem.Phys.* **2012**, *14*, 2239–2245.